


















Energetic Neutral Atom Fluxes from the Heliosheath: Constraints from in situ Measurements and Models

S. A. Fuselier^{1,2} , A. Galli³ , J. D. Richardson⁴ , D. B. Reisenfeld⁵ , E. J. Zirnstein⁶ , J. Heerikhuisen⁷ , M. A. Dayeh^{1,2} ,
N. A. Schwadron⁸ , D. J. McComas⁶ , H. A. Elliott^{1,2} , R. G. Gomez¹ , M. J. Starkey^{1,2} , M. Z. Kornbleuth⁹ ,
M. Opher⁹ , and K. Dialynas¹⁰ 

¹ Southwest Research Institute, San Antonio, TX, 78228, USA

² Department of Physics and Astronomy, University of Texas at San Antonio, San Antonio, TX, 78249, USA

³ Physics Institute, University of Bern, Bern, Switzerland

⁴ Massachusetts Institute of Technology, Cambridge, MA, USA

⁵ Los Alamos National Laboratory, ISR Division, Los Alamos, NM, 87545, USA

⁶ Department of Astrophysical Sciences, Princeton University, Princeton, NJ 08544, USA

⁷ Department of Mathematics and Statistics, University of Waikato, Hamilton, New Zealand

⁸ University of New Hampshire, Space Science Center, Durham, NH 03824, USA

⁹ Department of Astronomy, Boston University, Boston, MA, USA

¹⁰ Office of Space Research and Technology, Academy of Athens, Athens, Greece

Received 2020 December 9; revised 2021 May 22; accepted 2021 June 22; published 2021 July 8

Abstract

Voyager 2 observations throughout the heliosheath from the termination shock to the heliopause are used to normalize and constrain model pickup ion (PUI) fluxes. Integrating normalized PUI fluxes along the Voyager 2 trajectory through the heliosheath, and combining these integral fluxes with the energy-dependent charge-exchange cross section and the neutral hydrogen density, produces semi-empirical estimates of the energetic neutral atom (ENA) fluxes from the heliosheath. These estimated ENA fluxes are compared with observed ENA fluxes from the Interstellar Boundary Explorer (IBEX) to determine what percentage of the observed fluxes at each IBEX energy are from the heliosheath. These percentages are a maximum of $\sim 10\%$ for most energies and depend strongly on termination shock properties, plasma density, bulk plasma flow characteristics, the shape of the heliopause, and turbulent energy diffusion in the heliosheath.

Unified Astronomy Thesaurus concepts: [Astrosphere interstellar medium interactions \(106\)](#); [Solar wind \(1534\)](#); [Solar wind termination \(1535\)](#); [Interstellar medium \(847\)](#); [Pickup ions \(1239\)](#); [Space plasmas \(1544\)](#)

1. Introduction to the Heliosheath

The inner heliosheath, or simply the heliosheath, is the heliospheric region bounded by the termination shock (e.g., Richardson & Stone 2009) and the heliopause (e.g., Richardson et al. 2019). The radially expanding solar wind and pickup ions (PUIs) transition from supersonic to subsonic at the fast magnetosonic termination shock and enter the heliosheath. In the heliosheath, the bulk plasma flow is expected to be subsonic and this plasma continues to slow and deflect from the radial direction as it approaches the heliopause. The heliopause is the boundary of the heliosphere, where the outward-directed plasma and magnetic field pressure in the heliosheath balances the inward-directed interstellar plasma and magnetic field pressure in the local interstellar medium (LISM). However, for tens to hundreds of au beyond the heliopause, the heliospheric plasma and magnetic field still exert significant influence. For example, shocks from the heliosphere propagate into the LISM. Because of this influence, this part of the LISM has been called the outer heliosheath. Here, it is called simply the very LISM (VLISM).

Termination shock properties are strongly influenced by PUIs. The solar wind continuously charge-exchanges with incoming interstellar neutrals (ISNs) from the VLISM as it expands outward from the Sun. Observations from New Horizons (McComas et al. 2008) demonstrated that PUIs at ~ 38 au strongly dominate the total solar wind pressure (McComas et al. 2017). PUIs are a filled shell in velocity space with a shell radius of V_{SW} in the solar wind rest frame

(e.g., Vasyliunas & Siscoe 1976; McComas et al. 2017). Across the termination shock, theory indicates some general changes to this shell. PUIs should be decelerated by the cross-shock potential. The shell radius may increase by the shock compression ratio (Zank et al. 2010; Zirnstein et al. 2018a; Heerikhuisen et al. 2019; Shrestha et al. 2020) and there is reflection, energization, and return to the shock of a portion of the PUI population (e.g., Kumar et al. 2018). Beyond these general changes, the detailed changes of PUIs across the termination shock are still unclear.

There are no in situ observations of PUIs at the termination shock because Voyager 1 had no operating solar wind plasma instrument and Voyager 2 plasma observations were limited to the core solar wind. However, at the Voyager 2 crossing, the core solar wind did not transition from supersonic to subsonic and heated only adiabatically (Richardson et al. 2008). These observations, combined with the observed flow speed reduction of ~ 2.5 , indicate that most of the flow energy across the relatively strong shock likely went into PUIs and heating >28 keV ions (Decker et al. 2008; Richardson et al. 2008). An interplanetary shock with compression ratio ~ 3 observed by New Horizons showed similar preferential heating of PUIs compared to the core solar wind (Zirnstein et al. 2018b).

Voyager 2 was the first spacecraft to make solar wind plasma measurements across the entire heliosheath from the termination shock crossing in late 2007 to the heliopause crossing in late 2018 (see Figure 1(c)). The core solar wind slowed and heated approximately adiabatically downstream of the termination shock. Across most of the heliosheath, the plasma density

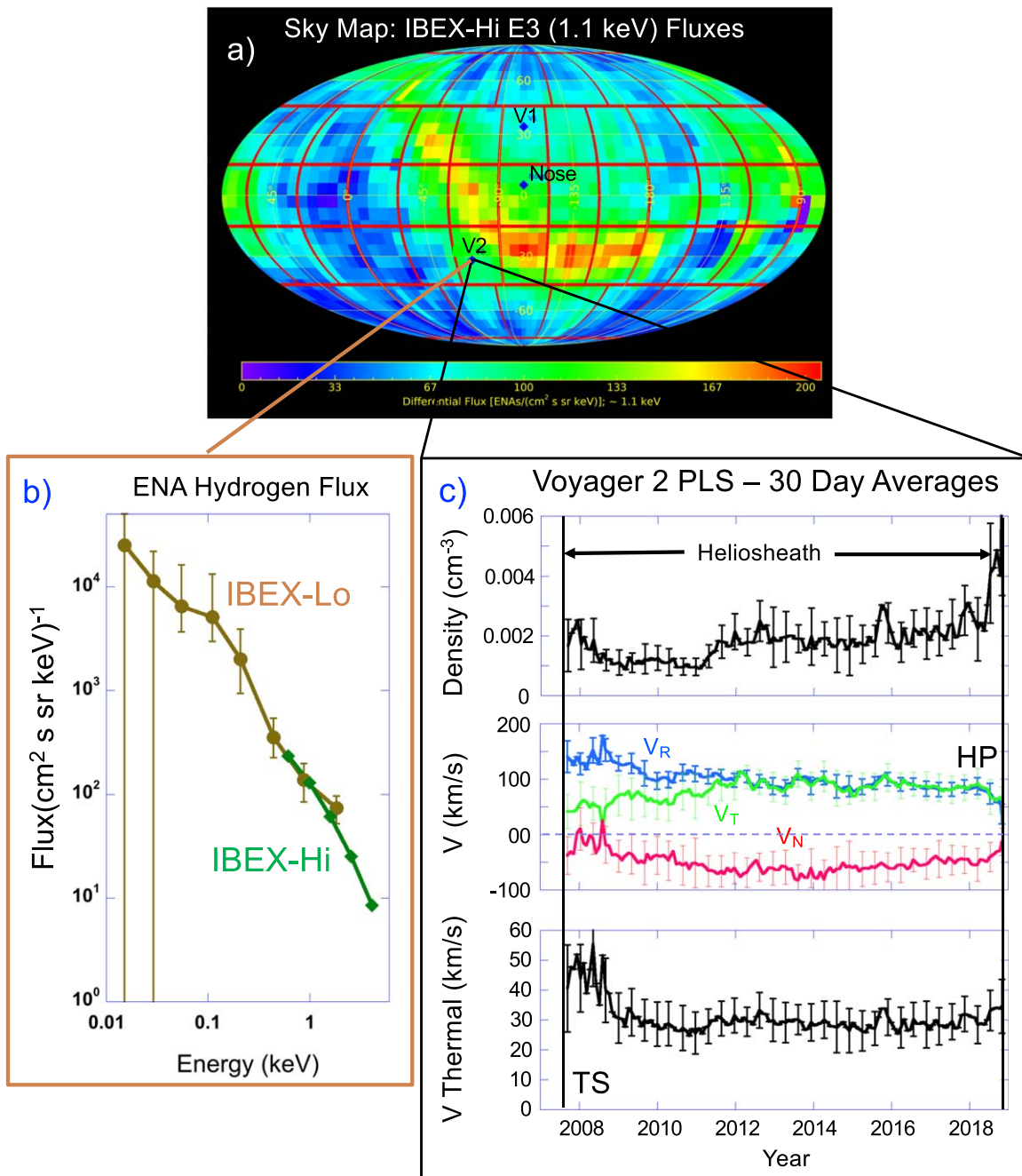


Figure 1. (a) All-sky Mollweide projection of 1.1 keV ENA fluxes from IBEX. The center of the map is the direction of the Sun’s motion relative to the Local Interstellar Cloud. The map is divided into macropixels and (b) shows the IBEX-Lo and -Hi energy spectrum from the pixel nearly centered on the Voyager 2 direction. (c) 30 day average density, three components of the velocity in RTN coordinates, and thermal velocity from the Voyager 2 Plasma Science (PLS) from the crossing of the termination shock in late 2007 to the heliopause crossing in late 2018. V_R and V_T decrease steadily through the heliosheath while V_N remains relatively constant. Just before the heliopause, the three components decrease more rapidly, but do not go to zero.

increased slowly by about a factor of 2 and the solar wind V_T and V_R were relatively constant. These velocity components decreased appreciably, but do not go to zero, as the heliopause was approached (Richardson et al. 2019). Throughout the heliosheath, the core solar wind temperature remained low and relatively constant (e.g., Richardson & Decker 2015).

The heliosheath is a source of ENAs produced by charge exchange of H^+ with ISNs (Krimigis et al. 2009; McComas et al. 2009a). These ENAs cover a broad energy range and propagate unimpeded by magnetic fields in all directions, including back into the inner heliosphere. They provide

information on three distinct PUI populations in the heliosheath: the transmitted, reflected (or energized), and injected PUI populations (Zirnstein et al. 2014; Heerikhuisen et al. 2019). The transmitted PUI population is produced in the supersonic solar wind and interacts with the termination shock as described above. The reflected or energized PUI population consists of PUIs that are reflected at the shock and returned to cross the shock. Finally, the injected PUI population is produced by charge exchange of core solar wind and PUIs with ISNs along the plasma flow streamlines from the

termination shock throughout the heliosheath. All PUIs may undergo further energy diffusion in the turbulent heliosheath.

Without other sources of ENAs, the ENA spectrum observed at 1 au by, e.g., the IBEX mission (McComas et al. 2009a), would be directly related to the line-of-sight-integrated solar wind and PUI populations in the heliosheath. However, the VLISM is another source of ENAs observed by IBEX, especially at energies less than about 3 keV, and particularly through the secondary ENA process (McComas et al. 2009b; Schwadron et al. 2009; Chalov et al. 2010; Heerikhuisen et al. 2010). This process likely produces the IBEX Ribbon as well as some fraction of the globally distributed flux (GDF; e.g., McComas et al. 2009b; Zirnstein et al. 2016; Desai et al. 2014).

The purpose of this Letter is to develop a semi-empirical estimate of the contributions of the heliosheath to IBEX ENA spectrum from the Voyager 2 direction. This estimate differs from previous estimates because Voyager 2 plasma observations provide in situ measurements of some plasma properties that are used in conjunction with two PUI models to determine ENA fluxes from the heliosheath.

2. ENA Fluxes from Plasma Observations and PUI Models

Figure 1 shows (a) IBEX global ENA observations at ~ 1.1 keV, (b) the ENA spectrum from the $30^\circ \times 30^\circ$ area in the sky that includes the Voyager 2 direction, and (c) the Voyager 2 in situ plasma observations in the heliosheath. The IBEX energy spectrum was integrated from 2009 through 2019, i.e., nearly the entire time that Voyager 2 was in the heliosheath. The low-energy ENA spectrum is from the IBEX-Lo sensor (Fuselier et al. 2009) and the high-energy spectrum is from the IBEX-Hi sensor (Funsten et al. 2009). The IBEX-Hi fluxes are from the latest data release (McComas et al. 2020), and all fluxes are Compton-Getting corrected for the motion of the Earth and IBEX around the Sun, and include the latest survivability correction for propagation from the heliosheath to 1 au. A large area in the sky and a long integration time were needed to get sufficient statistics for IBEX-Lo fluxes at low energies. Because this area includes an edge of the Ribbon (see Figure 1(a)), there is about a 10%–15% Ribbon contribution to the fluxes between 0.6 and 1 keV and negligible contribution to fluxes at other energies. This contribution was determined by separating the Ribbon and GDF using a process similar to that in Schwadron et al. (2018) and then computing the Ribbon contributions in each IBEX pixel and energy (Zimorino et al. 2019).

Equation (1) quantifies the relationship between ENA fluxes at a given energy, $J_{\text{ENA}}(E)$, and the integral along the radial line-of-sight of ion fluxes $J_{\text{ion}}(E, R)$ that are directed into the heliosphere. Charge exchange of these inward-directed ions produce ENAs with net velocities directed back to 1 au. In Equation (1), $n_H(R)$ is the ISN density and is assumed to be constant along the Voyager 2 trajectory at 0.12 cm^{-3} . The latest estimate for the ISN density at the termination shock is $0.127 \pm 0.015 \text{ cm}^{-3}$ (Swaczyna et al. 2020). Energy-dependent charge-exchange cross sections, $\sigma(E)$, are from Lindsay & Stebbings (2005). The heliosheath contribution to the observed ENA flux is determined by integrating Equation (1) using Voyager 2 observations and PUI models described below. The resulting ENA flux is compared to the observed IBEX ENA

flux.

$$J_{\text{ENA}}(E) = \int dR n_H(R) J_{\text{ion}}(E, R) \sigma(E) \quad (1)$$

Converting the integral into a sum along the Voyager trajectory, 60 day averages ($dR \sim 0.5$ au in Equation (1)) of the densities, radial and total velocities, and temperatures in Figure 1(c) characterize the core solar wind. These quantities are used to normalize PUI fluxes and temperatures that determine $J_{\text{ion}}(E, R)$ at the IBEX energies from 0.01 to 6 keV.

Two PUI models specify $J_{\text{ion}}(E, R)$. Two different models are used to emphasize different plasma processes and PUI populations that may contribute to ENA fluxes. The first model is called the Maxwellian model and is a multi-component suprathermal ion model that describes the core solar wind, transmitted PUIs, energized PUIs, and injected PUIs as Maxwellians (Heerikhuisen et al. 2019; Shrestha et al. 2020). This model is an extension of a three-component ion model (Zank et al. 2010) and has been used previously to describe the heliosheath ion distribution (Zirnstein et al. 2014), and to determine the ENA fluxes over a limited energy range (Zirnstein et al. 2014; Desai et al. 2014). All ion populations are co-moving with the core solar wind velocity and the temperature of the transmitted PUI population is consistent with the observed termination shock compression ratio of 2.5. Other model parameters are described in detail in case IV in Heerikhuisen et al. (2019). This model assumes sufficiently strong energy diffusion to produce Maxwellian transmitted and injected PUI populations along the flow streamlines from the termination shock to the Voyager 2 trajectory. The energy diffusion is not sufficient to produce a single Maxwellian for all PUI populations.

The second model is also a multi-component suprathermal ion model with the same solar wind and PUI populations as the first model; however, the transmitted PUI and injected PUI populations are filled shells in velocity space. Shell radii are determined from Voyager 2 observations as described below. The energized PUI population is a power law starting at the outer radius of the PUI shell. The $E^{-2.5}$ power law of this population is consistent with that observed downstream of relatively strong shocks (Starkey et al. 2019). Here, this model represents no energy diffusion, apart from the increase in the transmitted PUI shell radius across the termination shock.

Spacecraft observations are used to normalize the PUI parameters for the two model. The normalizations are similar, but have some important differences.

For the Maxwellian model, densities and temperatures of the core solar wind and PUI populations at three points along the Voyager 2 trajectory are from Heerikhuisen et al. (2019). Figure 2 shows a schematic of the Voyager 2 trajectory as it intersects heliosheath flow streamlines. Densities of all populations at these three points along the streamlines in Figure 2 are normalized by the ratio of the measured to modeled core solar wind density. The bottom panel of Figure 2 shows that the normalization factor is ~ 0.5 – 0.6 along most of the Voyager 2 trajectory except for the last ~ 4 au before the heliopause, where the factor is > 1 . All PUI populations are assumed to convect with the solar wind bulk velocity measured by Voyager 2. This assumption has important implications (see below). Below the schematic, the three components of the velocity from the model (in RTN coordinates) and the observed velocities are compared. When the error bars on the observed velocities are considered, the modeled and observed velocities

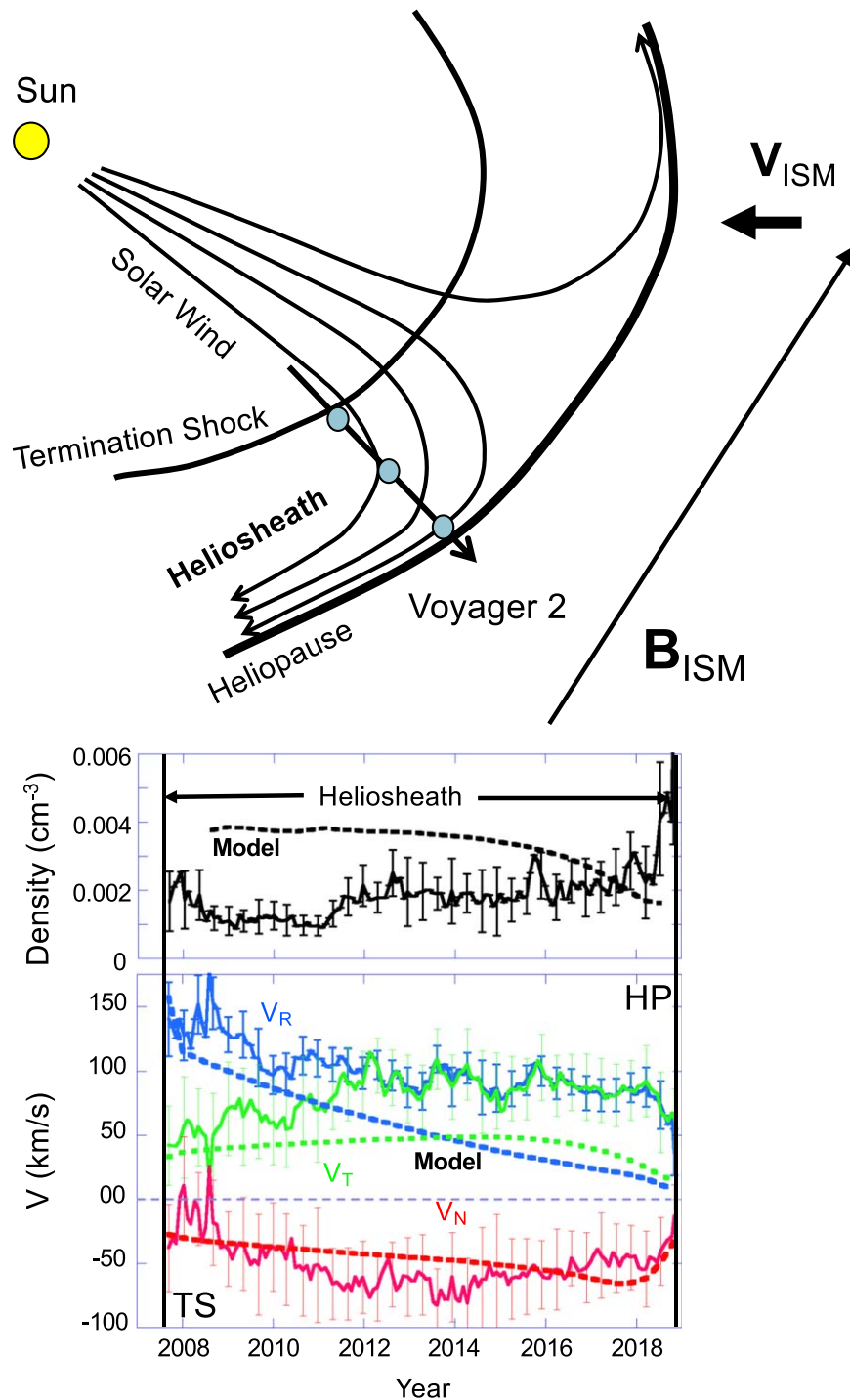


Figure 2. Top: schematic of Voyager 2’s trajectory through the heliosheath. All parameters in this qualitative schematic are projected into the meridional plane. Voyager 2 cuts across plasma streamlines that diverge from the position of maximum pressure exerted on the heliopause by the LISM. PUI parameters from a model are used from three locations in the heliosheath, near the termination shock (TS), mid-way through the heliosheath, and near the heliopause (HP) to determine the ENA flux from the Voyager 2 direction from the heliosheath. Bottom panel: comparison of the model densities and velocity components (dashed lines) and the Voyager 2 densities and velocities (data points with error bars) through the heliosheath. The observed and modeled densities differ by about a factor of 2 through most of the heliosheath. The observed radial and tangential velocities are higher than their respective model velocities through most of the heliosheath. The observed higher radial and tangential velocities have implications for the production of injected PUIs in the heliosheath.

compare reasonably well. However, important differences are that the observed tangential and radial velocities are relatively constant and consistently larger than their respective modeled velocities through most of the heliosheath. These differences have implications on the injected PUI density (see below).

Figure 2 also shows that the modeled heliosheath occurs at a radial distance between 75 and 112 au. Voyager 2 observed the termination shock (TS) at 84 au and a heliopause (HP) at 119 au. However, the critical parameter for the analysis here is the thickness of the heliosheath, which differs by only 2 au. PUI population temperatures and normalized densities are

linearly interpolated at locations separated by 60 days, or ~ 0.5 au along the Voyager trajectory.

For the Shell model, normalized densities of all populations are the same as those in the Maxwellian model. The transmitted PUI shell radius is 2.5 times the 350 km s^{-1} measured bulk solar wind velocity upstream of the TS. This radius is constant along the Voyager trajectory. The energized PUI population is an $E^{-2.5}$ power law starting at the radius of the transmitted PUI shell. The injected PUI shell radius is equal to the magnitude of the vector addition of the bulk velocity of the core solar wind measured by Voyager 2 and the 26 km s^{-1} ISN inflow velocity. For simplicity, the scalar sum is used, resulting in a shell radius about 10% larger than if the vector sum is used. Injected PUIs are assumed to be picked up and immediately scattered into a filled spherical shell with this radius. In general, these simplifying assumptions mean that the shell model may not conserve energy. The same linear interpolation of the parameters is performed as for the Maxwellian model.

Figure 3 shows cuts through the solar wind and PUI populations for the two models at three locations along the Voyager trajectory, near the TS, mid-way through the heliosheath, and near the HP. These cuts are along the radial flow direction and are in the solar inertial frame. In this frame, ions with negative velocities are the parent ions for IBEX ENA fluxes. For both models, the core solar wind is not the source of ENAs at any IBEX energy. This population is too cold and the outward radial velocity is too high to have a significant ion phase space density (PSD) at high, negative velocities. For the Maxwellian model, injected PUIs are parent ions for ENAs with $E < 0.2$ keV because the PSD is much higher than that of the transmitted PUI population in the second half of the heliosheath. Transmitted PUIs are parent ions for ENAs with $0.2 \text{ keV} < E < 2.6 \text{ keV}$. Energized PUIs are parent ions for ENAs with $E > 2.6$ keV. For the shell model, the transmitted PUIs are parent ions for all ENAs with $E < 2.6$ keV. The injected PUI shell radius is too small to provide significant PSD at high negative velocities, except at the lowest two IBEX-lo energies.

Ion fluxes along the Voyager trajectory were used in Equation (1) to compute ENA fluxes at the IBEX-Lo and -Hi energies. Figure 4 shows observed IBEX fluxes and computed ENA fluxes versus ENA energy. Computed fluxes are from Equation (1) using the two models versus ENA energy.

For the Maxwellian model, the heliosheath provides 4%–6% of the ENA flux for $E < 0.2$ keV. This percentage increases to $\sim 10\%$ at $E \sim 0.6$ keV and it remains approximately constant up to 6 keV. For the Shell model, the heliosheath provides $< 1\%$ of the ENA flux up to about $E \sim 0.5$ keV. It provides a steadily increasing percentage from 4% at 0.6 keV to 100% at 2.5 keV. Above 2.5 keV, the computed heliosheath ENA flux exceeds the measured IBEX flux.

3. Discussion

Equation (1) relates ENA fluxes with the line-of-sight integration of the neutral hydrogen density, ion fluxes, and charge-exchange cross sections. If it is assumed that the observed ENA flux comes entirely from the heliosheath, then the ENA flux provides important information on the PUI populations in the heliosheath and the outward-directed plasma pressure that balances the inward pressure from the VLISM. However, using two heliosheath PUI models, Figure 4 shows that contribution from the heliosheath to the ENA spectrum

with $E > 2$ keV is between 10% and 100% and the contribution to the ENA spectrum with $E < 1$ keV is never more than $\sim 10\%$. The obvious source for the remaining 90% ENAs at $E < 1$ keV is the VLISM. However, it is important to consider how modification of the heliosheath sources may result in a significant fraction of ENAs from the heliosheath.

The two PUI models represent two very different levels of ion energy diffusion in the heliosheath. For the transmitted and injected PUI populations, the Maxwellian model represents significant energy diffusion. In contrast, the Shell model represents no energy diffusion apart from the initial increase in the shell radius across the TS for the transmitted PUI population. Unfortunately, because the heliosheath plasma contributes so little to the observed ENA flux, little can be concluded about energy diffusion at the TS for the transmitted PUIs and in the heliosheath for the injected PUIs.

For $E > 2$ keV, Figure 4 shows that a high degree of energy diffusion results in a reduced contribution to the ENA spectrum from the heliosheath. Desai et al. (2014) arrived at a similar conclusion using shell-like and Maxwellian models. Recently, enhanced ENA fluxes at 4 keV were observed for a solar wind pressure pulse propagating through the heliosheath. The timing of these ENAs suggests that the dominant source for multi-keV ENAs is the heliosheath (McComas et al. 2018). Therefore, energy diffusion at $E > 2$ keV should be relatively slow. In fact, a recent model of stochastic acceleration of heliosheath PUIs (Zirnstein et al. 2018a) showed that a moderate amount of diffusion necessary to enhance ENA fluxes at $E < 2$ keV is not sufficient to diffuse ions near the filled shell cutoff at $E < 2$ keV.

Desai et al. (2014) and Zirnstein et al. (2014) also estimated the energy-dependent contributions to the ENA spectrum from the heliosheath in the Voyager direction using similar heliosheath models that produce similar flow streamlines (Heerikhuisen et al. 2019). These models all used similar values of n_H (see Equation (1)), but n_H was not constant through the heliosheath. It varied from $\sim 0.12 \text{ cm}^{-3}$ at the heliopause to $\sim 0.09 \text{ cm}^{-3}$ at the termination shock. Here, n_H was assumed to be constant at 0.12 cm^{-3} . Thus, the Desai et al. (2014), Zirnstein et al. (2014), and Heerikhuisen et al. (2019) had, on average, $\sim 15\%$ lower n_H density in heliosheath than assumed here. The estimates from Desai et al. (2014) and Zirnstein et al. (2014) differ somewhat from one another partly because Zirnstein et al. (2014) accounted for extinction of PUIs by charge exchange in the heliosheath. Despite this difference, contributions from the two models generally range from about 45% at $E \sim 0.3$ keV to $\sim 15\%$ at $E \sim 1.5$ keV. Thus, the semi-empirical model with the Voyager 2 constraints in Figure 4 produces ENA contributions that are a factor of 1.5–4.5 times smaller than that from the MHD models. Roughly half of the difference comes from using the Voyager 2 solar wind densities to normalize the PUI densities and another half comes from using the Voyager 2 velocities to determine the PUI populations in the solar inertial frame.

The use of Voyager 2 velocities to constrain the magneto-hydrodynamic (MHD) models is not a self-consistent procedure and has implicit, energy-dependent effects on the PUI populations in the heliosheath. The observed radial velocity along the Voyager 2 trajectory is consistently greater than the modeled radial velocity. A higher radial velocity along the plasma streamlines results in a lower production of injected PUIs and a higher survivability for transmitted PUIs. The

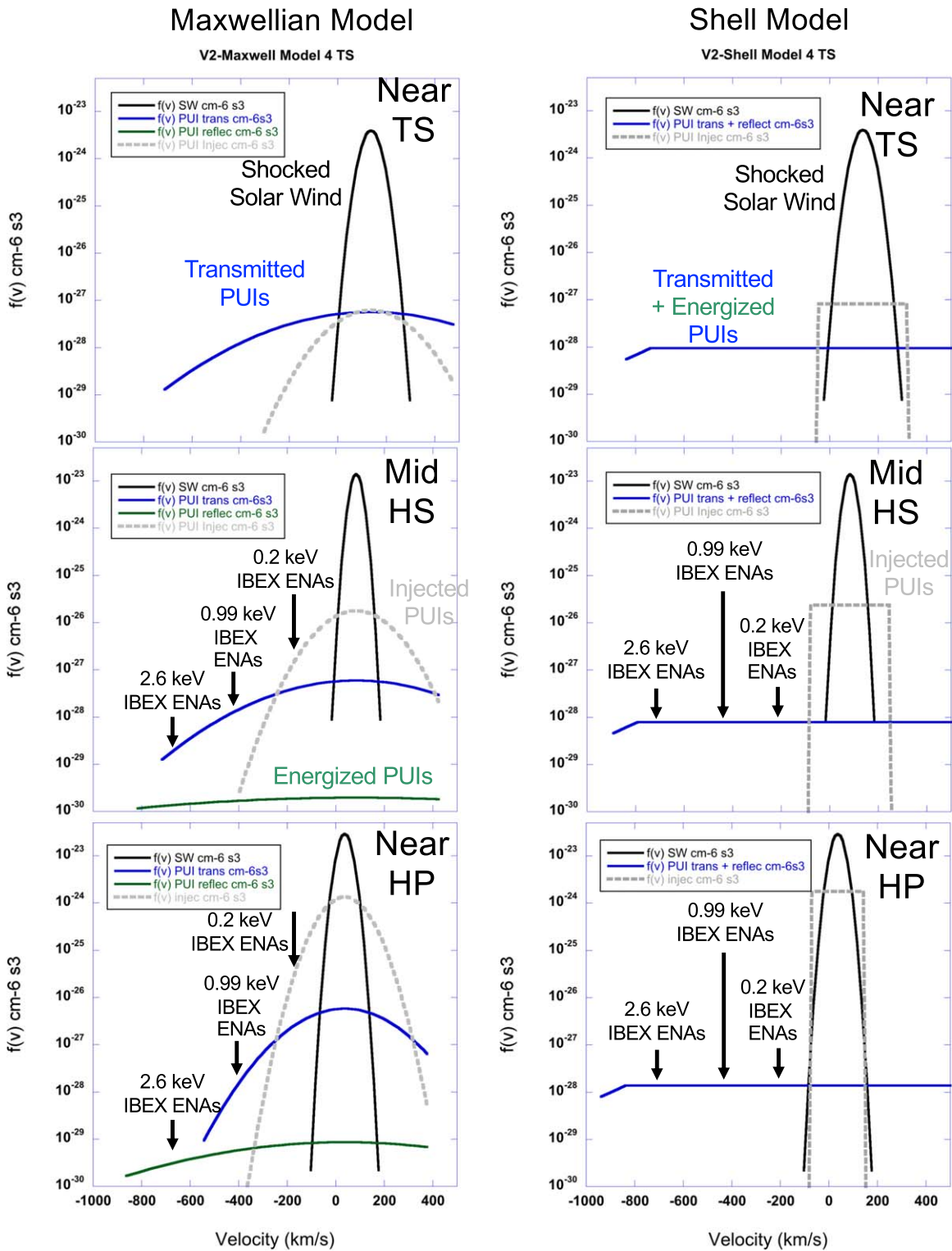


Figure 3. Shocked solar wind and PUI populations for the two models used to compute the ENA fluxes from the heliosheath. The ion phase space densities (PSDs) at negative velocities contribute to the ENA fluxes observed in the heliosphere at 1 au. For the Maxwellian model, injected PUIs contribute mainly to IBEX ENA fluxes at $E < 0.2$ keV, transmitted PUIs contribute mainly to ENA fluxes with $0.2 \text{ keV} < E < 2.6$ keV, and energized PUIs contribute mainly to ENA fluxes with $E > 2.6$ keV. For the shell model, injected PUI fluxes do not contribute to any IBEX ENA fluxes except for fluxes with $E < 0.02$ keV and transmitted PUIs contribute to ENA fluxes with $0.02 \text{ keV} < E < 2.6$ keV.

injected PUIs contribute to ENAs at $E < 0.3$ keV; therefore, ENA fluxes at $E < 0.3$ keV are likely overestimated. The survivability of the transmitted PUIs is estimated from Equations (2) and (3) in Zirnstein et al. (2014). Using the Voyager 2 velocities in Figure 1 to determine the relative

velocity between the transmitted PUIs and the interstellar neutrals, the survivability increases by approximately 35% over that determined using the model velocities in Figure 2. Thus, the ENA fluxes in Figure 4 at $E > 0.3$ keV are underestimated by a similar percentage. Nevertheless, the faster radial flow

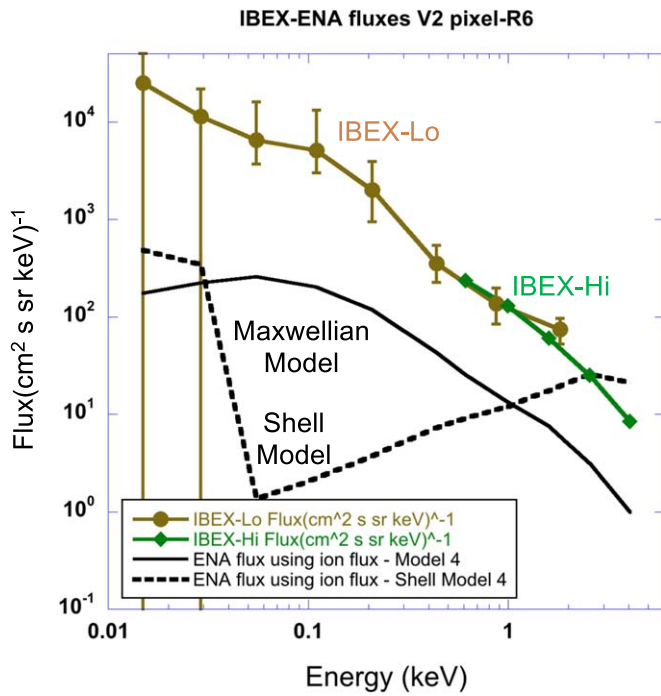


Figure 4. Observed ENA spectra from IBEX for the Voyager 2 pixel and predicted ENA fluxes from the two PUI models. The Maxwellian model produces a nearly continuous spectrum from $0.02 < E < 4$ keV dominated by contributions from injected PUIs with $E < 0.2$ keV and transmitted PUIs with $E > 0.2$ keV. Only $\sim 10\%$ of the ENAs with $E > 0.1$ keV are from the heliosheath. For the shell model, the contribution to the ENA spectrum from the heliosheath is negligible for ENAs with $E < 1$ keV.

observed by Voyager 2 yields a lower ENA flux than the MHD models predict.

The constraints applied here also depend strongly on the assumption that the time axis in Figure 1(c) represents spatial position in the heliosheath. This is equivalent to assuming that heliosheath boundaries are static for the 11 yr of the Voyager 2 heliosheath traversal. In contrast, simulations suggest that the TS could move 10 au in a few years (Izmodenov et al. 2008). The translation of time into spatial location has particular implications for radial and total velocities. Voyager 2 did not observe a substantial decrease in the radial velocity (Figure 1(c)) until at the HP (Richardson et al. 2019). If the HP was moving away from Voyager 2 in 2014–2017, then reversed and approached the spacecraft in 2018, then the observed radial velocity profile in Figure 1(c) and the modeled profile in Figure 2 do not represent a cut through the heliosheath and this velocity could be considerably lower in the outer half of the heliosheath. Low radial velocities in half of the heliosheath would imply substantially higher contribution to the ENA spectrum for $E < 1$ keV from the injected PUI population (see Figure 3).

A lower radial velocity also implies an increase in the streamline length as flows divert from radial to tangential (see Figure 2). Increased streamline length produces longer propagation times from the TS to the spacecraft and, therefore, produces more time to create injected PUIs through charge exchange. The increased propagation time should also increase the energy diffusion time via wave-particle turbulent interactions. Thus, the disparity between observed ENA flux for $E < 0.2$ keV and predicted flux from the inner heliosheath emphasizes the need to accurately model heliosheath plasma flows.

To further increase the heliosheath contribution to ENAs with $0.2 \text{ keV} < E < 1 \text{ keV}$, the modeled transmitted PUI flux must increase. Currently, the transmitted PUI density is $\sim 14\%$ of the core solar wind density. Until recently, the best estimate of the PUI density at the TS was also 14%, (McComas et al. 2017). However, new estimates, extrapolated from observations at 47 au, suggest that PUI densities at the TS are $\sim 24\%$ of the total density (McComas et al. 2021). Increasing the transmitted PUI density from 14% to 24% would increase the contribution to the ENA flux by a similar amount. Therefore, to increase the contribution to the ENA flux further, the form of the transmitted PUI distribution must change. One way to increase fluxes for $E < 1$ keV is to model the transmitted PUI population as a shell, but with a shell radius that is substantially less than 2.5 times the upstream solar wind velocity assumed in Figures 3 and 4 (Baliukin et al. 2020). A smaller shell radius would result in higher PSD at energies up to 1 keV for the Shell model in Figure 3. However, if this population participates in the shock structure, then the temperature of this population should increase by the compression ratio of 2.5 (Zank et al. 2010; Zirnstein et al. 2018a).

Other ways to increase the ENA flux for $0.2 \text{ keV} < E < 1 \text{ keV}$ are through stochastic acceleration of PUIs via turbulence (Zirnstein et al. 2018a, 2018c), reconnection (Opher et al. 2013), and PUI heating by interplanetary shocks propagating in the heliosheath (Mostafavi et al. 2019). These possibilities emphasize the importance of understanding the sources and extent of energy diffusion in the heliosheath, how the TS is mediated, and the complex linkage between macroscale, fluid flow streamlines in the heliosheath and microscale processes of energy dissipation at the TS and turbulent energy diffusion in the heliosheath.

Support for this study comes from the IBEX mission as a part of NASA’s Explorer program under grant 80NSSC20K0719. E.J.Z. also acknowledges support from NASA grant 80NSSC20K0783. IBEX is the result of efforts from a large number of scientists, engineers, and others. All who contributed to this mission share in its success. IBEX-Hi data in this Letter are from data release 16 and are available at <https://ibex.princeton.edu/DataRelease16>. Several of the authors were supported under NASA grant 18-DRIVE18_2-0029, Our Heliospheric Shield, 80NSSC20K0603. These authors also appreciate the candid discussions about the in situ and remote sensing observations, the macroscale and microscale processes in the heliosphere and LISM, and the size and shape of the heliosphere. The work at the Office for Space Research and Technology was supported by subcontracts at NASA (contracts NAS5 97271, NNX07AJ69G and NNN06AA01C). The New Horizons contribution was supported by NASW-02008.

ORCID iDs

S. A. Fuselier <https://orcid.org/0000-0003-4101-7901>
A. Galli <https://orcid.org/0000-0003-2425-3793>
J. D. Richardson <https://orcid.org/0000-0003-4041-7540>
D. B. Reisenfeld <https://orcid.org/0000-0003-1874-9450>
E. J. Zirnstein <https://orcid.org/0000-0001-7240-0618>
J. Heerikhuisen <https://orcid.org/0000-0001-7867-3633>
M. A. Dayeh <https://orcid.org/0000-0001-9323-1200>
N. A. Schwadron <https://orcid.org/0000-0002-3737-9283>
D. J. McComas <https://orcid.org/0000-0001-6160-1158>

H. A. Elliott  <https://orcid.org/0000-0003-2297-3922>
 R. G. Gomez  <https://orcid.org/0000-0001-7888-668X>
 M. J. Starkey  <https://orcid.org/0000-0001-7514-6571>
 M. Z. Kornbleuth  <https://orcid.org/0000-0002-3479-1766>
 M. Opher  <https://orcid.org/0000-0002-8767-8273>
 K. Dialynas  <https://orcid.org/0000-0002-5231-7929>

References

- Baliukin, I. I., Izmodenov, V. V., & Alexashov, D. B. 2020, *MNRAS*, **499**, 441
 Chalov, S. V., Alexashov, D. B., McComas, D., et al. 2010, *ApJ*, **716**, 99
 Decker, R. B., Krimigis, S. M., Roelof, E. C., et al. 2008, *Natur*, **454**, 67
 Desai, M. I., Allegrini, F. A., Bzowski, M., et al. 2014, *ApJ*, **780**, 98
 Funsten, H. O., Allegrini, F., Bochsler, P., et al. 2009, *SSRv*, **146**, 75
 Fuselier, S. A., Bochsler, P., Chormay, D., et al. 2009, *SSRv*, **146**, 117
 Heerikhuisen, J., Pogorelov, N. V., Zank, G. P., et al. 2010, *ApJL*, **708**, L126
 Heerikhuisen, J., Zirnstein, E. J., Pogorelov, N. V., et al. 2019, *ApJ*, **874**, 76
 Izmodenov, V. V., Malama, Y. G., & Ruderman, M. S. 2008, *AdSpR*, **41**, 318
 Krimigis, S. M., Mitchell, D. G., Roelof, E. C., Hsieh, K. C., & McComas, D. J. 2009, *Sci*, **236**, 971
 Kumar, R., Zirnstein, E. J., & Spitkovsky, A. 2018, *ApJ*, **860**, 156
 Lindsay, B. G., & Stebbings, R. F. 2005, *JGR*, **110**, A12213
 McComas, D. J., Allegrini, F., Bagenal, F., et al. 2008, *SSRv*, **140**, 261
 McComas, D. J., Allegrini, F., Bochsler, P., et al. 2009a, *SSRv*, **146**, 11
 McComas, D. J., Allegrini, F., Bochsler, P., et al. 2009b, *Sci*, **326**, 959
 McComas, D. J., Bzowski, M., Dayeh, M. A., et al. 2020, *ApJS*, **248**, 26
 McComas, D. J., Dayeh, M. A., Funsten, H. O., et al. 2018, *ApJL*, **856**, L10
 McComas, D. J., Swaczyna, P., Szalay, J. R., Zirnstein, E. J., et al. 2021, *ApJS*, **254**, 19
 McComas, D. J., Zirnstein, E. J., Bzowski, M., Elliott, H. A., et al. 2017, *ApJS*, **233**, 8
 Mostafavi, P., Zank, G. P., Zirnstein, E. J., et al. 2019, *ApJL*, **878**, L24
 Opher, M., Prested, C., McComas, D., et al. 2013, *ApJL*, **776**, L32
 Richardson, J. D., & Decker, R. B. 2015, *JPhCS*, **577**, 012021
 Richardson, J. D., & Stone, E. C. 2009, *SSRv*, **143**, 7
 Richardson, J. D., Belcher, J. W., Garcia-Galindo, P., & Burlaga, L. F. 2019, *NatAs*, **3**, 1019
 Richardson, J. D., Kasper, J. C., Wang, C., et al. 2008, *Natur*, **454**, 63
 Schwadron, N. A., Allegrini, F., Bzowski, M., et al. 2018, *ApJS*, **239**, 1
 Schwadron, N. A., Bzowski, M., Crew, G. B., et al. 2009, *Sci*, **326**, 966
 Shrestha, B. L., Zirnstein, E. J., & Heerikhuisen, J. 2020, *ApJ*, **894**, 102
 Starkey, M., Fuselier, S. A., Desai, M. I., et al. 2019, *GeoRL*, **46**, 10735
 Swaczyna, P., McComas, D. J., Zirnstein, E. J., et al. 2020, *ApJ*, in press
 Vasyliunas, V. M., & Siscoe, G. L. 1976, *JGR*, **81**, 1247
 Zank, G. P., Heerikhuisen, J., Pogorelov, N. V., Burrows, R., & McComas, D. J. 2010, *ApJ*, **708**, 1092
 Zimorino, A., Reisenfeld, D. B., & Funsten, H. O. 2019, AGU Fall Meeting 2019, abstract #SH51C-3339
 Zirnstein, E. J., Heerikhuisen, J., Funsten, H. O., et al. 2016, *ApJL*, **818**, L18
 Zirnstein, E. J., Heerikhuisen, J., Zank, G. P., et al. 2014, *ApJ*, **783**, 129
 Zirnstein, E. J., Kumar, R., Heerikhuisen, J., McComas, D. J., & Galli, A. 2018a, *ApJ*, **865**, 150
 Zirnstein, E. J., McComas, D. J., Kumar, R., et al. 2018b, *PhRvL*, **121**, 075102
 Zirnstein, E. J., Kumar, R., Heerikhuisen, J., et al. 2018c, *ApJ*, **860**, 170